Theoretical Chemistry Accounts (2020) 139:50
https://doi.org/10.1007/s00214-020-2563-6

REGULAR ARTICLE

The nature of the chemical bond in NO_3, neutral and anion

Apostolos Kalemos[1]

Received: 19 November 2019 / Accepted: 3 February 2020
© Springer-Verlag GmbH Germany, part of Springer Nature 2020

Abstract
The nitrate radical, NO_3, a molecular species of huge environmental importance has been an active research theme for at least a century at both the experimental and theoretical levels. Its ground-state symmetry, C_{2v} or D_{3h}, has puzzled the scientific community for nearly two decades, while its fascinating spectral profile is complicated due to intense vibronic couplings between its first five electronic states. In the present work, we report an elucidation of its chemical bonding based on a NO-*to*-NO_2-*to*-NO_3 formation sequence. We conclude that there are three different chemical bonds between N and the three O atoms, one double σ, π with an O (^{3}P), one dative σ with an excited O (~ ^{1}D) and finally a regular σ with a ground O (^{3}P). Its anion, NO_3^-, results naturally by grafting an additional electron to the ground neutral state.

Keywords Nature of chemical bond · Nitrate radical · Vibronic coupling

1 Introduction

The nitrate radical, NO_3, is one of the first polyatomic radicals to be discovered about 140 years ago in Paris of the *Belle Époque* [1, 2]. It is a major factor in the earth's atmosphere either by regulating ozone's depletion or by being responsible for the creation of a variety of harmful pollutants; see, e.g., Refs. [3–12].

Additionally, it represents one of the most exciting, extraordinary and complicated species in chemical physics that has been posing great challenges to both experimentalists and theoreticians. The major source of these fascinating problems is the intense vibronic coupling of Jahn–Teller (JT) or pseudo-JT character between its low-lying three (D_{3h})/five (C_{2v}) electronic states found within an energy range of 2 eV, namely $\tilde{X}^2A_2'/1^2B_2$, $\tilde{A}^2E''/1^2B_1$, 1^2A_2 and $\tilde{B}^2E'/1^2A_1$, 2^2B_2. Its intriguing characteristics have been the central theme of a great deal of high-quality work of both theoretical [13–38] and experimental [39–65] nature that continues up to the present [66, 67].

For nearly two decades, the question of whether its ground state is of C_{2v} or D_{3h} symmetry was a recurring theme of research; see, e.g., Refs. [13, 15, 18, 19, 21, 26], but finally the equilibrium geometry of this species was concluded to be of D_{3h} symmetry [21]. What is undoubtedly true is that the potential surface of its ground state is flat around its D_{3h} minimum along the planar asymmetric distortion, and the most interesting question we can really ask is what we can really learn from that fact. Or in other words what does the C_{2v}/D_{3h} rivalry teach us concerning the way three O atoms bind to N?

Another field of active research gears toward the spectroscopic characterization of its vibrational levels coupled together by various nonadiabatic couplings. This investigation path was initiated by Mayer et al. [20] who as early as 1993 tried to theoretically calculate the photoelectron spectrum of NO_3^-, obtained a few years earlier by Weaver et al. [44] through a multimode vibronic coupling model (KDC Hamiltonian) [68]. Weaver et al. observed directly and for the first time the first excited dark $\tilde{A}^2E''$ state, concluded on the D_{3h} symmetry of its ground state, and offered an extensive analysis of the vibronic coupling between $\tilde{X}^2A_2'$ and $\tilde{B}^2E'$ [44]. Its fascinating spectral profile has since been the subject of numerous theoretical *state-of-the-art* studies, see, e.g., Refs. [24–26, 28, 29, 32–38].

Despite the existence of so many theoretical studies on $\tilde{X}^2A_2'$, $\tilde{A}^2E''$ and $\tilde{B}^2E'$, there is still no answer on its bonding mechanism and this is exactly the sole purpose of the present paper. To this end, we have employed primarily the R(or U) CCSD(T) correlation method tailored for open-shell species

✉ Apostolos Kalemos
kalemos@chem.uoa.gr

[1] Department of Chemistry, Laboratory of Physical Chemistry, National and Kapodistrian University of Athens, Panepistimiopolis, Athens 157 71, Greece

Published online: 17 February 2020

coupled with the (aug-)cc-pVQZ basis sets [69]. Vibrational frequencies were calculated at the R(or U)CCSD(T)/cc-pVQZ level for the ground states of the NO_3 and NO_3^- species via numerical second derivatives. Additional information on computational aspects of this work will be given in due places throughout the text. Energy calculations were done with the MOLPRO code [70].

2 Results and discussion

With the goal of understanding the nature of the chemical bond in NO_3, we plan to trace its formation path through the NO-*to*-NO_2-*to*-NO_3 sequence. The ground NO state is of $X^2\Pi$ symmetry with its first excited $a^4\Pi$ state lying T_e= 38,440 cm^{-1} (= 110 kcal/mol) higher [71] (see also Table 1 for RCCSD(T)/cc-pVQZ values). Both states dissociate adiabatically to the ground-state fragments N (^{4}S) + O (^{3}P). Their CASSCF (11 valence electrons/8 valence orbitals) equilibrium wavefunctions and atomic Mulliken (NBO) populations are

$$\left|X^2\Pi\right\rangle \cong 0.96\left|1\sigma^2 2\sigma^2 3\sigma^2 1\pi_x^2 2\pi_x^1 1\pi_y^2\right\rangle \quad \text{with} \quad 1\sigma \sim 2s(\text{O}), \quad 2\sigma \sim 2s(\text{N}),$$
$$3\sigma \sim 0.71 \times 2p_z(\text{N}) - 0.74 \times 2p_z(\text{O}), \qquad 1\pi_x \sim 0.52 \times 2p_x(\text{N}) + 0.75 \times 2p_x(\text{O}),$$
$$2\pi_x \sim 0.88 \times 2p_x(\text{N}) - 0.70 \times 2p_x(\text{O}),$$
$$2s^{1.88}2p_x^{1.31}2p_y^{0.74}2p_z^{0.98}/_{\text{N}}2s^{1.80}2p_x^{1.64}2p_y^{1.22}2p_z^{1.29}/_{\text{O}}$$
$$\left(2s^{1.68}2p_x^{1.23}2p_y^{0.66}2p_z^{1.09}/_{\text{N}}2s^{1.74}2p_x^{1.75}2p_y^{1.32}2p_z^{1.43}/_{\text{O}}\right)$$

and

$$\left|a^4\Pi\right\rangle \cong 0.98\left|1\sigma^2 2\sigma^2 3\sigma^2 1\pi_x^2 2\pi_x^1 1\pi_y^1 2\pi_y^1\right\rangle \quad \text{with} \quad 1\sigma \sim 2s(\text{O}), 2\sigma \sim 2s(\text{N}),$$
$$3\sigma \sim 0.60 \times 2p_z(\text{N}) - 0.73 \times 2p_z(\text{O}), 1\pi_x \sim 0.30 \times 2p_x(\text{N}) + 0.91 \times 2p_x(\text{O}),$$
$$2\pi_x \sim 0.97 \times 2p_x(\text{N}) - 0.43 \times 2p_x(\text{O}), 2s^{1.93}2p_x^{1.13}2p_y^{1.0}2p_z^{0.86}/_{\text{N}}2s^{1.92}2p_x^{1.85}2p_y^{1.0}2p_z^{1.25}/_{\text{O}}$$
$$\left(2s^{1.85}2p_x^{1.08}2p_y^{1.0}2p_z^{0.88}/_{\text{N}}2s^{1.89}2p_x^{1.91}2p_y^{1.0}2p_z^{1.35}/_{\text{O}}\right).$$

Based on the above electronic characteristics, we can pictorially represent the $X^2\Pi$ and $a^4\Pi$ wavefunctions with the help of the valence bond Lewis (vbL) diagrams shown in Schemes 1 and 2.

The odd electron is hosted by an orbital with greater amplitude on N, and the $X^2\Pi$-to-$a^4\Pi$ transformation is accomplished through the rupture of the π_y bond. The addition of an H (^{2}S) atom creates HNO ($\tilde{X}^1A'$) but not NOH since the odd electron appears to be more localized on the N atom; see Table 1 for energies and molecular parameters. There is thus a double (σ, π) bond between N and O and a single bond between N and H (H–N=O). The latter (N–H) bond features a binding energy of D_e = 52.7 kcal/mol with respect to NO ($X^2\Pi$) + H (^{2}S) at the RCCSD(T)/cc-pVQZ computational level. Most interesting though is the addition of OH ($X^2\Pi$) to form nitrous acid, HO–N=O. It has a planar (C_s) structure of $\tilde{X}^1A'$ symmetry with its RCCSD(T)/cc-pVQZ equilibrium parameters presented in Table 1. There is again a double (σ, π) bond between N and the terminal O atom and a single bond between N and the hydroxyl O atom (HO–N=O).

If we now consider H–N=O($\tilde{X}^1A'$) and approach an O atom, we will get an isomer of nitrous acid, the H–NO_2 [$\tilde{X}^1A_1(C_{2v})$] species where the H atom is now attached to N. Adiabatically, H–NO_2($\tilde{X}^1A_1$) follows the HNO ($\tilde{a}^3A''$) + O (^{3}P) fragmentation path rather than HNO ($\tilde{X}^1A'$) + O (^{1}D) since T_e ($\tilde{a}^3A'' \leftarrow \tilde{X}^1A')_{\text{HNO}}$ = 19.3 kcal/mol (Table 1) and ΔE ($^1\text{D} \leftarrow {}^3\text{P})_{\text{O}}$ = 45.1 kcal/mol [72]; see Fig. 1 for the CASSCF (18 valence electrons/13 valence orbitals) interaction curves, but the HNO ($\tilde{a}^3A''$; $\pi_x^1\pi_y^1$) + O (^{3}P; $2p_x^1p_z^1$) electronic distribution does not lead to any chemical bonding. Hopefully enough, the interaction with the HNO ($\tilde{X}^1A'$) + O ($2p_x^2p_y^2$; ~ ^{1}D) distribution comes into rescue at around 5.0 bohr by creating a dative bond between the ~ $2s^2$(N) electronic density and the "empty" ~ $2p_z$(O) orbital. Proof of that is the equilibrium Mulliken (NBO) population $2s^{1.30}$ ($2s^{1.16}$) of nitrogen and the Mulliken charges on each O atom, q = −0.26 (−0.32). This population decline of the 2*s*(N) density reflects exactly the formation of a dative bond and that its minimum correlates adiabatically to HNO ($\tilde{X}^1A'$) + O (~^{1}D). After a careful inspection of the evolution of the CASSCF wavefunction and molecular orbitals along the reaction coordinate, we come up with the following equilibrium C_{2v} structure represented pictorially by the vbL diagram of Scheme 3.

Table 1 Energies E (hartree) and molecular parameters (bond distances in Å and bond angles in degrees) of the different species studied in the present work at the RCCSD(T)/cc-pVQZ computational level

Species	$-E$	Molecular parameters				
NO($X^2\Pi$)	129.754 228	1.152_{NO}				
NO($a^4\Pi$)	129.579 560	1.421_{NO}				
HNO($\tilde{X}^1A'$)	130.338 133	1.211_{NO}	1.053_{NH}	$108.0_{\angle ONH}$		
HNO($\tilde{a}^3A''$)	130.307 335	1.218_{NO}	1.026_{NH}	$120.2_{\angle ONH}$		
HONO($\tilde{X}^1A'$)	205.497 705	$1.422_{HO\text{-}NO}$	$1.171_{HON\text{-}O}$	0.965_{HO}	$110.7_{\angle ONO}$	$102.0_{\angle HON}$
HNO_2($\tilde{X}^1A_1$)	205.485 069	1.217_{NO}	1.034_{NH}	$128.2_{\angle ONO}$	$115.9_{\angle HNO}$	
NO_2($\tilde{X}^2A_1$)	204.862 081	1.195_{NO}	$134.2_{\angle ONO}$			
NO_2($\tilde{A}^2B_2$)	204.814 133	1.258_{NO}	$101.2_{\angle ONO}$			
NO_2($\tilde{B}^2\Pi_u$)	204.797 862	1.201_{NO}				
NO_2($\tilde{C}^2A''$)	204.786 491	1.167_{NO_1}	1.498_{NO_2}	$109.6_{\angle O_1NO_2}$		
NO_2($\tilde{C}^2A_2$)	204.783 327	1.275_{NO}	$109.9_{\angle ONO}$			
NO_3($\tilde{X}^2A_2'$)	279.930 737	$1.233^a_{NO_{1,2,3}}$	$120.0_{\angle ONO}$			
NO_3($\tilde{A}^2E''$)	279.888 325	$1.261^a_{NO_{1,2,3}}$	$120.0_{\angle ONO}$			
NO_3($\tilde{A}^2B_1$)	279.902 927	$1.424^a_{NO_1}$	$1.204_{NO_{2,3}}$	$114.7^a_{\angle O_1NO_{2,3}}$	$130.6_{\angle O_2NO_3}$	
NO_3($\tilde{A}^2A_2$)	279.895 105	$1.202^a_{NO_1}$	$1.293_{NO_{2,3}}$	$123.8^a_{\angle O_1NO_{2,3}}$	$112.5_{\angle O_2NO_3}$	
NO_3($\tilde{B}^2E'$)	279.857 994	$1.266^a_{NO_{1,2,3}}$	$120.0_{\angle ONO}$			
NO_3($\tilde{B}^2A_1$)	279.860 328	$1.236^a_{NO_1}$	$1.283_{NO_{2,3}}$	$118.3^a_{\angle O_1NO_{2,3}}$	$123.3_{\angle O_2NO_3}$	

[a]NO_1 defines the C_2 axis of the C_{2v} point group

At the CASSCF equilibrium geometry, the wavefunction of the H–NO_2 ground state is dominated ($C_0 = 0.95$) by the $(1-10)a'^2(1-2)a''^2$ electronic configuration characteristic of the HNO ($\tilde{X}^1A'$) + O (^{1}D) asymptote while the open singlet character of the HNO ($\tilde{a}^3A''$) + O (^{3}P) channel passes through to the second and third $^1A'$ states. The upshot of the above discussion is that there is a double (σ, π) N=O bond, a single dative N → O bond and a plain single N–H bond in H–NO_2, where one of the O atoms is found in situ in its excited ~ ^{1}D (actually a mixture of ^{1}D and ^{1}S) state and the other in its ground ^{3}P one, while in nitrous acid, HO–N=O, both O atoms are found in their ^{3}P ground states.

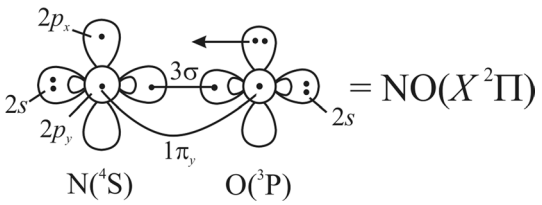

Scheme 1 vbL diagram of NO ($X^2\Pi$)

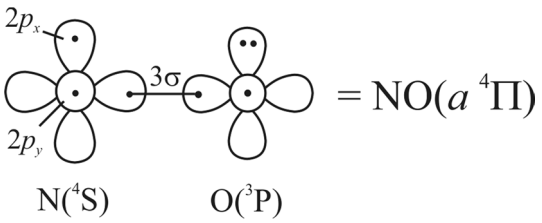

Scheme 2 vbL diagram of NO ($a^4\Pi$)

At this point, it is informative to compare H–NO_2 to the isoelectronic and isovalent O_3 species since NH ($X^3\Sigma^-$) is

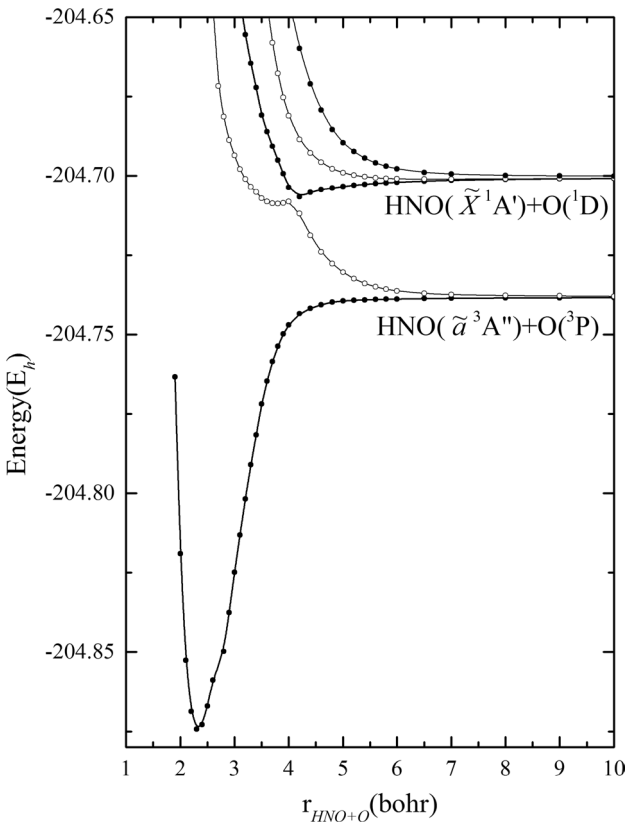

Fig. 1 SACASSCF/cc-pVQZ potential energy curves ($^1A'$) of the planar HNO + O interaction. The HNO unit features the equilibrium parameters of the ground HNO_2 species

Scheme 3 vbL diagram of the ground HNO_2 state

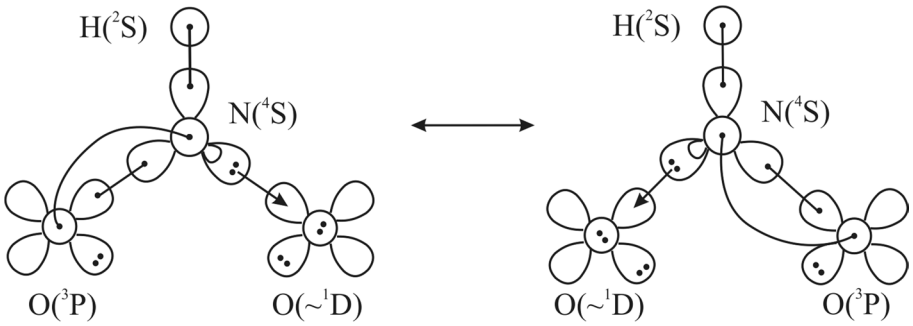

isoelectronic and isovalent to O (^{3}P). As we have already shown [73, 74], the $\tilde{X}^1A'O_3$ state is bound by a double (σ, π) bond and a single dative bond between the central and the terminal O atoms, as is the case between NH and the two terminal O atoms in H–NO_2.

In order to decipher the chemical bond in NO_3 we should first understand NO_2 and the way it is formed. NO_2 is a notoriously difficult molecule with both an academic and environmental interest. It has been the subject of numerous theoretical studies during the last 50 years, see, e.g., Refs. [75–91]. It has a rich and complicated electronic spectrum primarily due to conical intersections. A recent synoptical presentation of the problems encountered in its study can be found in Ref. [91]. The focus of the NO_2 research is on its first four electronic states of $\tilde{X}^2A_1$, $\tilde{A}^2B_2$, $\tilde{B}^2B_1(^2\Pi_u)$ and $\tilde{C}^2A''$ symmetry with potential energy minima within an energy range of 2 eV; see Table 1 for RCCSD(T)/cc-pVQZ theoretical results. Its basic ingredient is clearly NO ($X^2\Pi$) that features a regular σ and π bonds (see Scheme 1). A second O atom can approach either in its ground ^{3}P or its first excited ^{1}D state. The bent $\tilde{X}^2A_1$ NO_2 state becomes a $^2\Pi_u$ linear state. So, how can one form a linear ONO ($^2\Pi_u$) state from NO ($X^2\Pi$) + O? The answer is shown in Fig. 2 that displays the CASSCF (17 valence electrons/12 valence orbitals) potential curves of the NO ($X^2\Pi$) + O (^{3}P or ^{1}D) interaction. The NO ($X^2\Pi$) + O (^{3}P) attack is clearly repulsive, and this is expected on the basis of its asymptotic configuration, that is NO ($X^2\Pi$) + O (^{3}P; $2p_x^1 2p_y^1 2p_z^2$). But the NO ($X^2\Pi$) + O (^{1}D) attack is attractive due to the dative σ bond between the $2s^2$(N) and O ($2p_x^2 2p_y^2$; ~ ^{1}D) distributions. The Mulliken (NBO) population of the nitrogen $2s^{1.20}$ ($2s^{1.15}$) orbital and the −0.17 (−0.36) Mulliken (NBO) charge on the O atoms reflect once again the dative nature of the bonding mechanism. Graphically, it is described by Scheme 4.

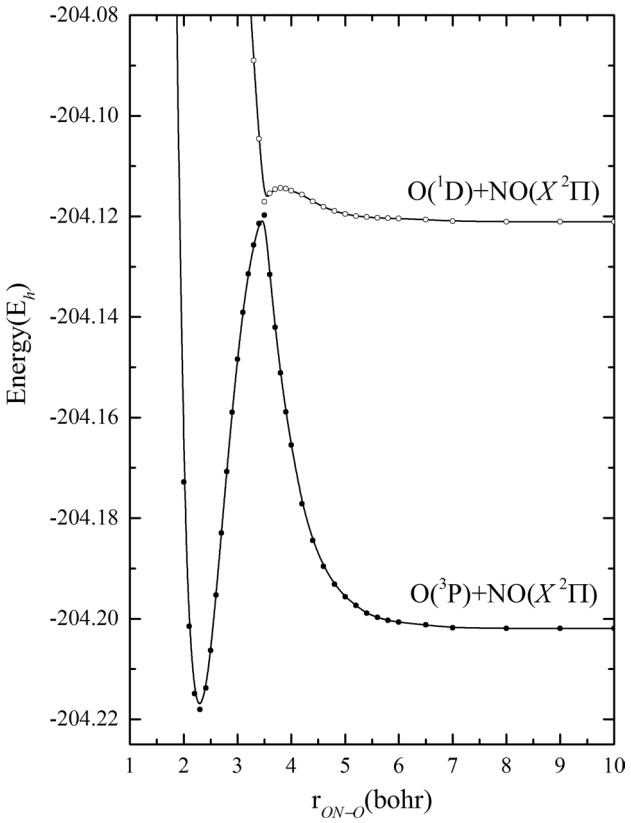

Fig. 2 SACASSCF/cc-pVQZ potential energy curves ($^2\Pi$) of the linear NO + O interaction. The minimum of the lowest curve is of $^2\Pi_u$ symmetry, while NO features the distance as found in ONO ($X^2\Pi_u$)

By bending it, we get NO_2 ($\tilde{X}^2A_1$) with CASSCF (17 valence electrons/12 valence orbitals) equilibrium characteristics

$$\left|\tilde{X}^2A'(\tilde{X}^2A_1)\right\rangle \cong 0.94\left|(1-9)a'^2 10a'^1 (1-2)a''^2\right\rangle \quad \text{with}$$

$$10a' \sim -0.36 \times 2s(\mathrm{N}) - 0.32 \times s'(\mathrm{N}) + 0.64 \times 2p_z(\mathrm{N}) - 0.58 \times [2p_z(\mathrm{O}_1) + 2p_z(\mathrm{O}_2)],$$

and atomic populations (Mulliken) $2s^{1.47}2p_x^{1.0}2p_y^{0.84}2p_z^{1.18}/_{\mathrm{N}}2s^{1.83}2p_x^{1.45}2p_y^{1.29}2p_z^{1.55}/_{\mathrm{O}_{1,2}}$

and (NBO) $2s^{1.22}2p_x^{0.87}2p_y^{0.94}2p_z^{1.20}/_{\mathrm{N}}2s^{1.76}2p_x^{1.55}2p_y^{1.39}2p_z^{1.62}/_{\mathrm{O}_{1,2}}$.

Scheme 4 vbL diagram of the linear ONO ($^2\Pi_u$) configuration

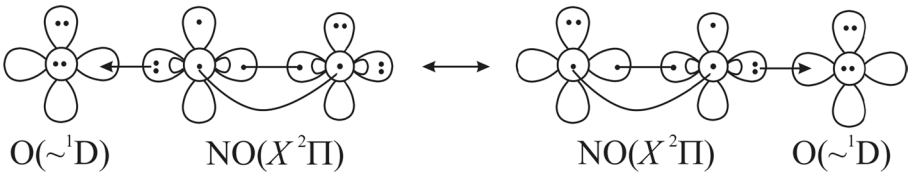

Scheme 5 vbL diagram of the ground NO_2 state

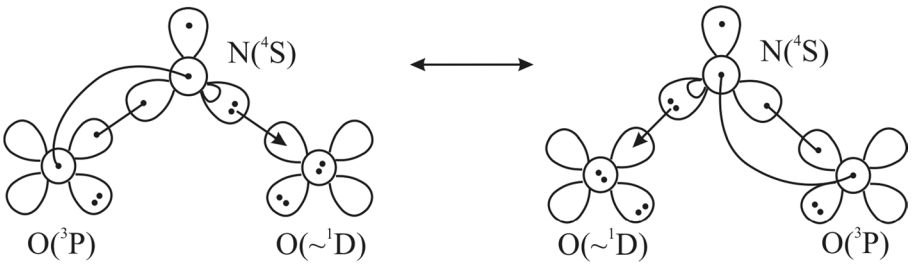

Scheme 6 vbL diagram of the first excited ($\tilde{A}^2B_2$) NO_2 state

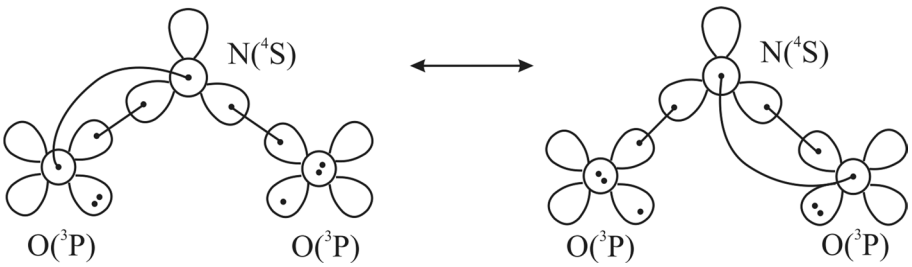

The NO_2 ($\tilde{X}^2A_1$) state is mainly described graphically by Scheme 5.

The above analysis is also in agreement with the bonding characteristics of the H–NO_2 (←HNO + O) species discussed above.

The first excited $\tilde{A}^2B_2$ state with CASSCF (17 valence electrons/12 valence orbitals) equilibrium characteristics

$$\left|\tilde{A}^2A'(\tilde{A}^2B_2)\right\rangle \cong 0.92\left|(1-9)a'^2 10a'^1(1-2)a''^2\right\rangle \quad \text{with}$$

$$10a' \sim 0.62\times[2p_y(O_1)+2p_y(O_2)] - 0.43\times[2p_z(O_1)-2p_z(O_2)]$$

has its in-plane odd electron localized on the O atoms, and this can happen from the NO ($X^2\Pi$) + O (^{3}P) bent interaction as also analyzed in the planar ON–OH case (see above) and depicted graphically in Scheme 6.

It is clear that nitrous acid, HO–NO (110.7°$_{\angle ONO}$; Table 1), traces its diabatic lineage to the $\tilde{A}^2B_2$ NO_2 (101.2°$_{\angle ONO}$; Table 1) state while H–NO_2 (128.2°$_{\angle ONO}$; Table 1) to $\tilde{X}^2A_1$ NO_2 (134.2°$_{\angle ONO}$; Table 1). There is also a number of well-known chemical species that relate to NO_2 ($\tilde{X}^2A_1$). These are O_2N–NO_2 (135°$_{\angle ONO}$), HO–NO_2 (130°$_{\angle ONO}$), ON–NO_2 (130°$_{\angle ONO}$) and H_2N–NO_2 (130°$_{\angle ONO}$) [92]. In all of the above species, the ONO angle is practically identical to the one in the ground NO_2 state and there is a single bond between NO_2 and the incoming ligand. The most interesting case is nitric acid, HO–NO_2, featuring one σ bond between HO($X^2\Pi$) and NO_2 ($\tilde{X}^2A_1$), a double (σ, π) and a dative σ bond between N and the terminal O atoms. It has a planar C_s structure with its RCCSD(T)/cc-pVQZ molecular parameters appearing in Scheme 7.

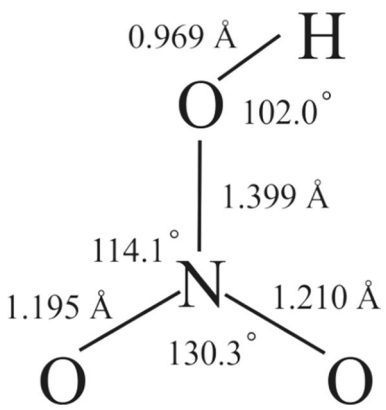

Scheme 7 Molecular parameters of the ground HNO_3 state at the RCCSD(T)/cc-pVQZ computational level

By detaching the H atom, we get a $^2A'$ NO_3 species that becomes its $\tilde{X}^2A_2'$ state upon geometry optimization. So, the

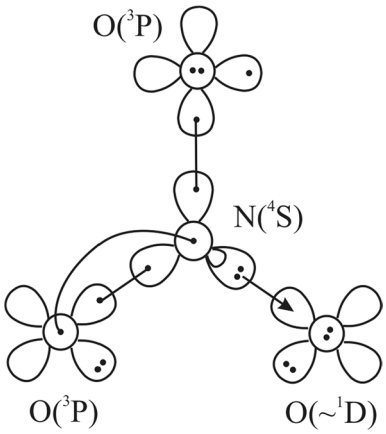

Scheme 8 vbL diagram of NO_3 ($^2A'$)

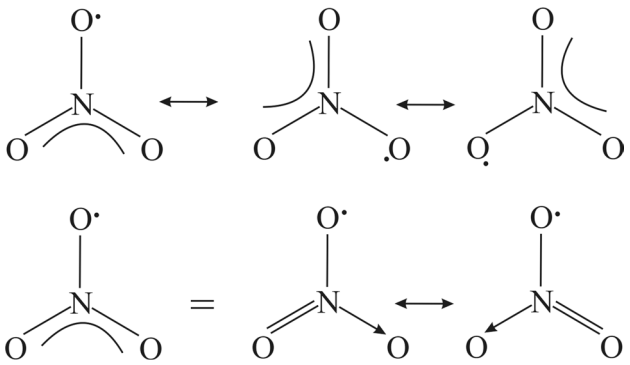

Scheme 9 Resonant vbL structures of the ground NO_3 state

generic type of bonding in the ground NO_3 state is captured by the vbL diagram of Scheme 8.

There are three different chemical bonds in NO_3, a regular ($2e^- - 2$ center) σ, a dative σ and a double σ, π, while the odd electron rests on a single O atom. Once again, the Mulliken (NBO) population and charges $2s_N^{1.19}$ ($2s_N^{1.05}$) and $q(O) = -0.21$ (-0.29), $q(N) = +0.64$ ($+0.88$) mirror the character of the chemical bond. The equilateral symmetry dictates similar vbL structures in which the odd electron can be found on all three O atoms that upon interaction confer it a D_{3h} equilibrium structure. This is graphically represented by the vbL diagram shown in Scheme 9.

The addition of an H atom destroys the above resonance, the wave function collapses into one of the three vbL structures, and the electron localizes on a particular O atom, and thus, we get a (quasi)C_{2v}(H)O–NO_2 unit featuring one long and two short NO distances as found also in previous studies [13]. Thus, the D_{3h} structure of the ground NO_3 species is due to the resonance of all the vbL structures shown in Scheme 9.

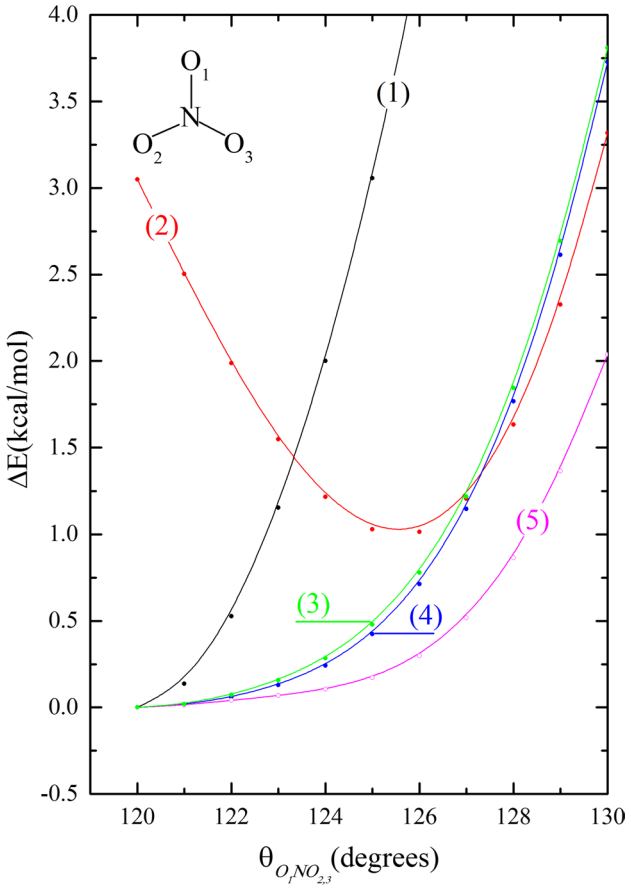

Fig. 3 (R or U)CCSD(T)/cc-pVQZ potential energy curves (PEC) of the ground NO_3 species along the θ (O_1NO_2=O_1NO_3) coordinate. At each energy point, the NO distances are optimized. PEC_(1) (black) and _(2) (red) are obtained at the ROHF(NO_3)–RCCSD(T) level featuring a D_{3h} and C_{2v} energy minima, respectively, while PEC_(3) (green), _(4) (blue) and _(5) (magenta) at the ROHF(NO_3^-)–UCCSD(T), ROHF(NO_3^-)–RCCSD(T) and ROHF(NO_3)–UCCSD(T), respectively. The latter three PECs have been shifted so that their minima coincide to PEC_(1)'s minimum (see Table 2 for absolute energies)

The symmetry breaking problem of the $\tilde{X}^2A_2'$ state is illustrated in Fig. 3 that displays RCCSD(T) and UCCSD(T) potential energy curves along the θ (O_1NO_2=O_1NO_3) coordinate based on ROHF orbitals of either the neutral NO_3 or anionic NO_3^- species. PEC_(1) and PEC_(2) are based on two different ROHF(NO_3) solutions that produce curves with either D_{3h} (see Table 2) or C_{2v} ($E_e = -279.929\ 146\ E_h$, r_e (NO_1) = 1.197 Å, r_e ($NO_{2,3}$) = 1.258 Å, θ (O_2NO_3) = 108.9°, ω_e = 504, 636, 797, 1082, 1199, 1596 cm^{-1}) energy minima, respectively. Both D_{3h} and C_{2v} structures are chemical entities that should be considered evenly in order to accurately map the adiabatic surface of the ground NO_3 state and it appears that ROHF(NO_3)–UCCSD(T) or ROHF(NO_3^-)–(R or U)CCSD(T) computational schemes are suitable for that.

Table 2 Energies E (hartree), bond distances r_e (Å), harmonic frequencies ω_e (cm^{-1}) and electron affinity EA (eV) of the ground D_{3h} $\tilde{X}^2A_2'$ (NO_3) and $\tilde{X}^1A'$ (NO_3^-) states at the ROHF-(R or U)CCSD(T)/(aug)-cc-pVQZ computational level

Species	$-E$	r_e	ω_e (q_4, q_2, q_1, q_3)	EA
$NO_3(\tilde{X}^2A_2')$	279.930 737[a]	1.233[a]	614 (b_2, a_1), 793 (b_1), 1106 (a_1), 1497 (b_2, a_1)[a]	
	279.931 433[b]	1.234[b]	280 (b_2, a_1), 793 (b_1), 1107 (a_1), 1131 (b_2, a_1)[b]	
	279.929 216[c]	1.233[c]	263 (b_2, a_1), 794 (b_1), 1108 (a_1), 1162 (b_2, a_1)[c]	
	279.929 970[d]	1.233[d]	289 (b_2, a_1), 794 (b_1), 1108 (a_1), 1171 (b_2, a_1)[d]	
			369 (b_2, a_1), 764 (b_1), 1067 (a_1), 1099 (b_2, a_1)[e]	
			388 (b_2, a_1), 808 (b_1), 1095 (a_1), 1067 (b_2, a_1)[f]	
			349 (b_2, a_1), 773 (b_1), 1085 (a_1), 1140 (b_2, a_1)[g]	
			361 (b_2, a_1), 1051 (a_1), 994 (b_2, a_1)[h]	
			237 (b_2, a_1), 793 (b_1), 1155 (a_1), 1412 (b_2, a_1)[i]	
		[1.24][j]	[365(b_2, a_1),[k] 762 (b_1),[k] 1051(a_1),[l] (b_2, a_1)[m]]	
	(279.940 813)	(1.234)		
$NO_3^-(\tilde{X}^1A')$	280.073 084	1.255	717 (b_2, a_1), 859 (b_1), 1066 (a_1), 1423 (b_2, a_1)	3.87
			[723 (b_2, a_1), 834 (b_1), 1054 (a_1), 1379 (b_2, a_1)][n]	
	(280.090 367)	(1.257)		(4.07)
		[1.23][n]		[3.937 ± 0.014][n]

Experimental results in square brackets

[a]ROHF(NO_3)–RCCSD(T) results, see also PEC_(1) in Fig. 3

[b]ROHF(NO_3)–UCCSD(T) results, see also PEC_(5) in Fig. 3

[c]ROHF(NO_3^-)–RCCSD(T) results, see also PEC_(4) in Fig. 3

[d]ROHF(NO_3^-)–UCCSD(T) results, see also PEC_(3) in Fig. 3

[e]Scaled results based on a MSCAS(17e$^-$/13o)PT2/aug-cc-pVTZ surface; unscaled ones are 392, 733, 1066 and 1162 cm^{-1}, Ref. [33]

[f]EOMIP-CCSD/[3*s*2*p*1*d*] results based on the adiabatic approximation, Ref. [29]

[g]UCCSD(T)/ADZ results, Ref. [27]

[h]Results based on the KDC Hamiltonian and on EOMIP-CCSD/cc-pVTZ ab initio energy points, Ref. [26]

[i]MRCISD/AVTZ-f; MRCISD + Q results are 273, 773, 1083 and 1376 cm^{-1}, Ref. [23]

[j]References [41, 42]

[k]Reference [61]

[l]References [39, 40]

[m]1087 $cm^{-1} \le \omega_3 \le 1127$ cm^{-1}, see Ref. [58], $\omega_3 = 1492$ cm^{-1}, see, e.g., Ref. [64] and $\omega_3 = 1044(16)$ cm^{-1}, see Ref. [93]

[n]Reference [42]

The above two "structures" lie in the heart of the C_{2v}/D_{3h} problem of the past.

It is interesting to comment on the behavior of the harmonic frequencies according to the computational schemes used (see Table 2). Although the ω_2 and ω_1 values are practically equal at all levels of theory employed, this is not the case for ω_3 and ω_4. The computational schemes that take into account both D_{3h} and C_{2v} minima (PEC_(3, 4, 5)) give values that are much closer to the experimental and some previous theoretical values. It turns out that the latter ω_3 values (see Table 2) are closer to the experimental expectation $1087 \le \omega_3 \le 1127$ cm^{-1} (see Ref. [58]) and to the KDC value of 1069 cm^{-1} (see Ref. [29]) than the 1492 cm^{-1} value (see Ref. [64]). Based on our bonding analysis and the form of the potential curves, we believe that the ~ 1000 cm^{-1} should be the correct one. And this is indeed the case as shown recently by the high-resolution photoelectron spectroscopy

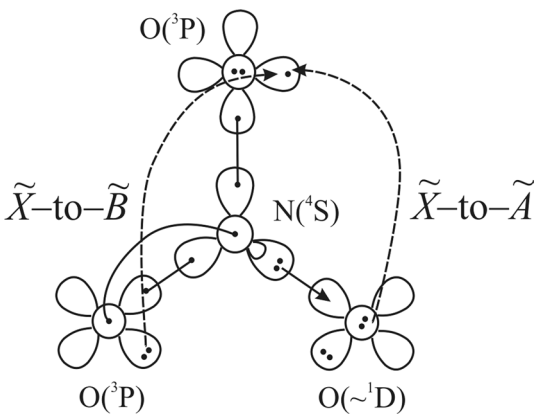

Scheme 10 vbL diagram of the (generic) electronic excitations from the ground to the first and second excited NO_3 states

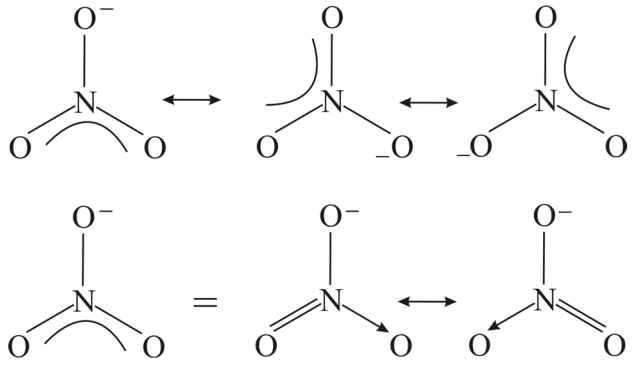

Scheme 11 Resonant vbL structures of the ground NO_3^- state

of cryogenically cooled NO_3^- establishing a value of 1044(16) cm^{-1} [93].

Now that we understand the bonding nature of the ground NO_3 state, it is a not a difficult task to delve into the bonding character of its excited $\tilde{A}^2E''(1^2B_1, 1^2A_2)$ and $\tilde{B}^2E'$ $(1^2A_1, 2^2B_2)$ states. Under $D_{3h}(C_{2v})$ symmetry labeling, the $\tilde{A}^2E''(^2A_2$ or $^2B_1)$ state is realized through an $e''(a_2$ or $b_1)$ $\rightarrow a_2'(b_2)$ transition, while the $\tilde{B}^2E'(^2A_1$ or $^2B_2)$ state is realized through an $e'(a_1$ or $b_2) \rightarrow a_2'(b_2)$ excitation. Considering also the composition of the out-of-plane (e'')/in-plane (e') (NO_3) molecular orbitals, we can easily visualize the $\tilde{X}^2A_2' \rightarrow \tilde{A}^2E''/\tilde{B}^2E'$ transitions with the help of the C_s bonding motif shown in Scheme 10.

The resulting $\tilde{A}^2E''$ and $\tilde{B}^2E'$ states are Jahn–Teller active and give rise to C_{2v} structures of 1^2B_1, 1^2A_2 and 1^2A_1, 2^2B_2 symmetry, respectively; see Table 1 for their molecular parameters. In the 1^2B_1 state [T_e= 6104 cm^{-1}; 7062.25(50) cm^{-1} (exp. T_0 value, see, e.g., Refs. [44] and [60])], the π electron is localized on the O atom that defines the C_2 axis while in the 1^2A_2 state on the two equivalent O atoms. In the $\tilde{B}$ states [T_e (1^2A_1) = 15,453 cm^{-1}; 15,109 cm^{-1} (exp. T_0 value, see, e.g., Ref. [51])], the in-plane odd electron is on $2p_y 2p_z$ hybrids of the two equivalent O atoms.

Based on Scheme 8, we can easily understand the chemical structure of NO_3^-. The negative charge finds its way into the half-occupied O orbital. The Mulliken (NBO) population and charges $2s_N^{1.24}$ $(2s_N^{1.05})$ and $q(O) = -0.54$ (-0.63), $q(N) = +0.61$ $(+0.89)$ are in agreement with the bonding situation. The additional electron is shared equally (1/3 = 0.33) by all O atoms as witnessed by the Mulliken charges of the neutral $(q(O) = -0.21)$ and anion $(q(O) = -0.54)$, while that of N remains unaltered (see the vbL diagram of Scheme 11).

Its molecular parameters and its harmonic frequencies appear in Table 2. The computed electron affinity EA = 3.87 (4.07) eV at the RCCSD(T)/(aug)-cc-pVQZ computational level is in fair agreement with the experimental value of 3.937 ± 0.014 eV [44]. Interestingly enough, the EA value at the ROHF(NO_3^-)–RCCSD(T)/(cc-pVQZ computational level EA = 3.91 eV is in much closer agreement with the experimental one.

3 Conclusions

The nitrate radical, NO_3, is a notoriously difficult species both in terms of bonding and of its spectral behavior complicated by various nonadiabatic couplings. All of its peculiarities should be traced back to the way the three O atoms bind to nitrogen. And this is exactly the subject matter of the present study. We have followed a NO-*to*-NO_2-*to*-NO_3 formation path and have shown that the equilateral equilibrium structure of its ground $\tilde{X}^2A_2'$ state is due to the resonance of vbL structures, each one of them featuring three different chemical bonds between N and O, one double σ, π with an O (^{3}P), one dative σ with an excited O (~ ^{1}D) and finally a regular σ with a ground O (^{3}P). The presence of an H atom (in HO–NO_2) breaks the resonance of the NO_3 unit conferring it a (quasi) C_{2v} character. An additional electron finds its place into the "hole" of the neutral radical, and consequently the anion features a similar D_{3h} structure.

References

1. Chappuis J (1882) Ann Sci ENS 11:137–186
2. Hautefeuille P, Chappuis J (1881) C R Acad Sci Paris 92:80
3. Atmospheric Ozone 1985: assessment of our understanding of the processes controlling its present distribution and change, World Meteorological Organization, Global Ozone Research and Monitoring Project-Report No. 16 (NASA, Washington DC, 1985), pp 32–35
4. Johnston HS, Podolski J (1978) Rev Geophys Space Phys 16:491–519
5. Seinfield H (1989) Science 243:745–752
6. Wayne RP, Barnes I, Biggs P, Burrows JP, Canosa-Mas CE, Hjorth JE, LeBras G, Moortgat GK, Perner D, Poulet G, Restelli G, Sidebottom H (1991) Atmos Environ 25A:1–203
7. Wayne RP (1991) Chemistry of atmospheres. Clarendon, Oxford
8. Platt U, Perner D, Winer AM, Harris GW, Pitts JV Jr (1980) Geophys Res Lett 7:89–92
9. Noxon JF, Norton RB, Marovich E (1980) Geophys Res Lett 7:125–128
10. Platt U, Heinz F (1994) Isr J Chem 34:289–300
11. Atkinson R (2000) Atmos Environ 34:2063–2101
12. Monks PS (2005) Chem Soc Rev 34:376–395
13. Siegbahn PEM (1985) J Comput Chem 6:182–188
14. Boehm RC, Lohr LL (1989) J Phys Chem 93:3430–3433
15. Davy RD, Schaefer HF III (1989) J Chem Phys 91:4410–4411
16. Kaldor U (1990) Chem Phys Lett 166:599–601
17. Kim B, Hammond BL, Lester WA, Johnston HS (1990) Chem Phys Lett 168:131–134
18. Stanton JF, Gauss J, Bartlett RJ (1991) J Chem Phys 94:4084–4087
19. Stanton JF, Gauss J, Bartlett RJ (1992) J Chem Phys 97:5554–5559
20. Mayer M, Cederbaum LS, Köppel H (1994) J Chem Phys 100:899–911
21. Eisfeld W, Morokuma K (2000) J Chem Phys 113:5587–5597
22. Cohen RD, Sherrill CD (2001) J Chem Phys 114:8257–8269

23. Eisfeld W, Morokuma K (2001) J Chem Phys 114:9430–9440
24. Viel A, Eisfeld W (2004) J Chem Phys 120:4603–4613
25. Mahapatra S, Eisfeld W, Köppel H (2007) Chem Phys Lett 441:7–15
26. Stanton JF (2007) J Chem Phys 126:134309
27. Glendening ED, Halpern AM (2007) J Chem Phys 127:164307
28. Faraji S, Köppel H, Eisfeld W, Mahapatra S (2008) Chem Phys 347:110–119
29. Stanton JF (2009) Mol Phys 107:1059–1075
30. Stanton JF, Okumura M (2009) Phys Chem Chem Phys 11:4742–4744
31. Grein F (2013) J Chem Phys 138:204305
32. Eisfeld W, Vieuxmaire O, Viel A (2014) J Chem Phys 140:224109
33. Homayoon Z, Bowman JM (2014) J Chem Phys 141:161104
34. Mukherjee B, Mukherjee S, Sardar S, Shamasundar KR, Adhikari S (2017) Mol Phys 115:2833–2848
35. Mukherjee B, Mukherjee S, Adhikari S (2017) J Phys Chem A 121:6314–6326
36. Eisfeld W, Viel A (2017) J Chem Phys 146:034303
37. Viel A, Eisfeld W (2018) Chem Phys 509:81–90
38. Mukherjee B, Mukherjee S, Sardar S, Shamasundar KR, Adhikari S (2018) Chem Phys 515:350–359
39. Nelson HH, Pasternack L, McDonald JR (1983) J Phys Chem 87:1286–1288
40. Ishiwata T, Fujiwara L, Naruge Y, Obi K, Tanaka I (1983) J Phys Chem 87:1349–1352
41. Ishiwata T, Tanaka I, Kawaguchi K, Hirota E (1985) J Chem Phys 82:2196–2205
42. Friedl RR, Sander SP (1987) J Phys Chem 91:2721–2726
43. Kawaguchi K, Hirota E, Ishiwata T, Tanaka I (1990) J Chem Phys 93:951–956
44. Weaver A, Arnold DW, Bradforth SE, Neumark DM (1991) J Chem Phys 94:1740–1751
45. Monks PS, Stief LJ, Krauss M, Kuo SC, Zhang Z, Klemm RB (1994) J Phys Chem 98:10017–10022
46. Kawaguchi K, Ishiwata T, Tanaka I, Hirota E (1991) Chem Phys Lett 180:436–440
47. Kawaguchi K, Ishiwata T, Hirota E, Tanaka I (1998) Chem Phys 231:193–198
48. Ishiwata T, Tanaka I, Kawaguchi K, Hirota E (1992) J Mol Spectrosc 153:167–180
49. Wang D, Jiang P, Qian X, Hong G (1997) J Chem Phys 106:3003–3006
50. Kim BS, Hunter PL, Johnston HS (1992) J Chem Phys 96:4057–4067
51. Carter RT, Schmidt KF, Bitto H, Huber JR (1996) Chem Phys Lett 257:297–302
52. Hirota E, Ishiwata T, Kawaguchi K, Fujitake M, Obashi V, Tanaka I (1997) J Chem Phys 107:2829–2838
53. Okumura M, Stanton JF, Deev A, Sommar J (2006) Phys Scr 73:C64–C70
54. Hirota E, Kawaguchi K, Ishiwata T, Tanaka I (1991) J Chem Phys 95:771–775
55. Nelson HH, Pasternack L, McDonald JR (1983) J Chem Phys 79:4279–4284
56. Jacox ME, Thompson WE (2008) J Chem Phys 129:204306
57. Jacox ME, Thompson WE (2010) J Phys Chem A 114:4712–4718
58. Kawaguchi K, Shimizu N, Fujimori R, Tang J, Ishiwata T, Tanaka I (2011) J Mol Spectrosc 268:85–92
59. Simmons CS, Ichino T, Stanton JF (2012) J Phys Chem Lett 3:1946–1950
60. Takematsu K, Eddingsaas NC, Robichaud DJ, Okumura M (2013) Chem Phys Lett 555:57–63
61. Fujimori R, Shimizu N, Tang J, Ishiwata T, Kawaguchi K (2013) J Mol Spectrosc 283:10–17
62. Kawaguchi K, Fujimori R, Tang J, Ishiwata T (2013) J Phys Chem A 117:13732–13742
63. Tada K, Kashihara W, Baba M, Ishiwata T, Hirota E, Kasahara S (2014) J Chem Phys 141:184307
64. Hirota E (2015) J Mol Spectrosc 310:99–104
65. Codd T, Chen M-W, Roudjane M, Stanton JF, Miller RA (2015) J Chem Phys 142: 184305
66. Tada K (2019) Chem Phys 524:21–25
67. Sharma K, Garner S, Miller TA, Stanton JF (2019) J Phys Chem A 123:4990–5004
68. Köppel H, Domcke W, Cederbaum LS (1984) Adv Chem Phys 57:59–246
69. Dunning TH Jr (1989) J Chem Phys 90:1007–1023
70. MOLPRO is a package of ab initio programs written by Werner H-J, Knowles PJ, Knizia G, Manby FR, Schütz M, Celani P, Györffy W, Kats D, Korona T, Lindh R, Mitrushenkov A, Rauhut G, Shamasundar KR, Adler TB, Amos RD, Bernhardsson A, Berning A, Cooper DL, Deegan MJO, Dobbyn AJ, Eckert F, Goll E, Hampel C, Hesselmann A, Hetzer G, Hrenar T, Jansen G, Köppl C, Liu Y, Lloyd AW, Mata RA, May AJ, McNicholas SJ, Meyer W, Mura ME, Nicklaß A, O'Neill DP, Palmieri P, Peng D, Pflüger K, Pitzer R, Reiher M, Shiozaki T, Stoll H, Stone AJ, Tarroni R, Thorsteinsson T, Wang M (2008) MOLPRO, version 2012.1, a package of ab initio programs. University College Cardiff Consultants Limited, Cardiff
71. Huber KP, Herzberg G (1979) Constants of diatomic molecules (data prepared by J.W. Gallagher and R.D. Johnson, III). In: Linstrom PJ, Mallard WG (eds) NIST Chemistry WebBook, NIST Standard Reference Database Number 69. National Institute of Standards and Technology, Gaithersburg. https://doi.org/10.18434/t4d303
72. Kramida A, Ralchenko Y, Reader J, NIST ASD Team (2018) NIST atomic spectra database (ver. 5.6.1), https://physics.nist.gov/asd. National Institute of Standards and Technology, Gaithersburg. https://doi.org/10.18434/T4W30F
73. Kalemos A, Mavridis A (2008) J Chem Phys 129:054312
74. Kalemos A (2016) J Phys Chem A 120:169–170
75. Hay PJ (1973) J Chem Phys 58:4706–4707
76. Jackels CF, Davidson ER (1975) J Chem Phys 63:4672–4677
77. Jackels CF, Davidson ER (1976) J Chem Phys 64:2908–2917
78. Jackels CF, Davidson ER (1976) J Chem Phys 65:2941–2957
79. Shih S-K, Peyerimhoff SD, Buenker RJ (1977) Chem Phys Lett 46:201–207
80. Xie Y, Davy RD, Yates BF, Blabous CP III, Yamaguchi Y, Schaefer HF III (1989) Chem Phys 135:179–186
81. Blabous CP III, Yates BF, Xie Y, Schaefer HF III (1990) J Chem Phys 93:8105–8109
82. Burton NA, Yamaguchi Y, Alberts IL, Schaefer HF III (1991) J Chem Phys 95:7466–7478
83. Crawford TD, Stanton JF, Szalay PG, Schaefer HF III (1997) J Chem Phys 107:2525–2528
84. Mahapatra S, Köppel H, Cederbaum LS, Stampfuß P, Wenzel W (2000) Chem Phys 259:211–226
85. Kurkal V, Fleurat-Lessard P, Schinke R (2003) J Chem Phys 119:1489–1501
86. Varandas AJC (2003) J Chem Phys 119:2596–2613
87. Bera PP, Yamaguchi Y, Schaefer HF III (2007) J Chem Phys 127:174303
88. Grein F (2008) Chem Phys Lett 455:124–130
89. Mota VC, Caridale PJSB, Varandas AJC (2012) J Phys Chem A 116:3023–3034
90. Sardar S, Mukherjee S, Paul AK, Adhikari S (2013) Chem Phys 416:11–20
91. Mukherjee S, Mukherjee B, Sardar S, Adhikari S (2015) J Chem Phys 143:244307

92. Greenwood NN, Earnshaw A (1997) Chemistry of the elements, 2nd edn. Butterworth-Heinemann, Oxford
93. Babin MC, DeVine JA, DeWitt M, Stanton JF, Neumark DM (2020) J Phys Chem Lett 11:395–400

Publisher's Note Springer Nature remains neutral with regard to jurisdictional claims in published maps and institutional affiliations.